CHARGED PARTICLE RADIATION DAMAGE IN SEMICONDUCTORS, X:

THE ENERGY DEPENDENCE OF ELECTRON DAMAGE IN SILICON

3 SEPTEMBER 1964

4161-6004-KU-000

Contract NAS5-3805
NATIONAL AERONAUTICS AND SPACE ADMINISTRATION
GODDARD SPACE FLIGHT CENTER

TRW SPACE TECHNOLOGY LABORATORIES
THOMPSON RAMO WOOLDRIDGE INC.

CHARGED PARTICLE RADIATION DAMAGE IN SEMICONDUCTORS, X:

THE ENERGY DEPENDENCE OF ELECTRON DAMAGE IN SILICON

3 SEPTEMBER 1964

4161-6004-KU-000

Contract NAS5-3805
NATIONAL AERONAUTICS AND SPACE ADMINISTRATION
GODDARD SPACE FLIGHT CENTER

TRW SPACE TECHNOLOGY LABORATORIES
THOMPSON RAMO WOOLDRIDGE INC.

TABLE OF CONTENTS

Page

I. INTRODUCTION 1

II. DESCRIPTION OF EXPERIMENTS 2

Test Specimens 2
Measurements 3
Dosimetry 8
Experimental Techniques 10
Pre-irradiation Experiments 11

III. EXPERIMENTAL RESULTS 11

Degradation of Solar Cell Output Characteristics. 12
Radiation Induced Energy Levels in Silicon 25

IV. SUMMARY AND CONCLUSIONS. 34

LIST OF ILLUSTRATIONS

		Page
1	Typical Minority Carrier Diffusion Length Degradation Data	14
2	Typical I-V Characteristic Degradation Data	15
3	Typical Short Circuit Current Degradation Data	17
4	Electron Energy Dependence of K Values for P on N Silicon Solar Cells	18
5	Electron Energy Dependence of Φ_c^{-1} Values for P on N Silicon Solar Cells	19
6	Electron Energy Dependence of K Values for N on P Silicon Solar Cells	21
7	Electron Energy Dependence of Φ_c^{-1} Values for N on P Silicon Solar Cells	22
8	Degradation of Open Circuit Voltage as a Function of Resistivity	24
9	Degradation of Maximum Power Under Solar Illumination as a Function of Resistivity	26
10	Dependence of Minority Carrier Lifetime Degradation on Resistivity	28
11	Dependence of Lifetime on Reciprocal Temperature	30
12	Dependence of Lifetime on Reciprocal Temperature	31
13	Electron Energy Dependence of the $E_t - E_v = 0.3$ev Defect Level in 150 ohm-cm P-Type Silicon	33
14	Electron Energy Dependence of the $E_c - E_t = 0.17$ev Defect Level in 100 ohm-cm N-Type Silicon	35

Table I - Φ_c and K Values as a Function of Energy of Solar Cell Type 13

I. INTRODUCTION

Because of the importance of electrons in the energy range of 1 Mev and above, a series of experiments were conducted in February and March of 1963 to compare the experimentally observed electron energy dependence with theoretical predictions based on classical relativistic Coulomb scattering laws and simple displacement theory. These experiments, conducted at the General Atomic linear electron accelerator facilities in San Diego, indicated that p on n silicon solar cells and gallium arsenide solar cells agreed quite well with the theoretical predictions[1,2]. However, n on p silicon solar cells were observed to exhibit damage rates greatly in excess of those predicted by theory as a function of increasing electron energy. Although the data obtained in these initial experiments confirmed the steep energy dependence of electron radiation damage for n on p silicon solar cells, the data were not adequate for accurate power supply design calculations due to lack of sufficient statistical data and lack of information on the dependence of this effect on base material resistivity. In addition, an insufficient number of specimens were obtained for laboratory study in the determination of the energy levels and defect mechanisms responsible for the observed departure from existing theory.

Due to the increasing use of the more radiation-resistant n on p high resistivity silicon solar cells in the construction of satellite solar cell power supply systems, a third series of experiments were performed in May 1964 at the General Atomic linear electron accelerator facilities. The objectives of this third series of experiments were: (1) to obtain statistically significant and accurate data on the energy dependence of electron radiation damage, (2) to determine the effect of resistivity on the damage rate and energy dependence, and (3) to obtain added specimens and information for further analysis of the energy levels and defect mechanisms responsible

for electron radiation damage in silicon. The purpose of this paper is the presentation of the results of these experiments. The next section describes the conduct of the experiments; Section III presents the results and analysis of the data, and Section IV presents the conclusions based on the data obtained in this series of experiments.

II. DESCRIPTION OF EXPERIMENTS

In this section a description of the experiments and experimental techniques will be presented. Subjects to be covered include the description of the test specimens, the measurements performed before, during, and after the experiments, the beam diagnostics used to determine the radiation environment, and the techniques used to analyze the data and determine the energy dependence of the damage characteristics.

Test Specimens

The test specimens consisted of both p on n and n on p silicon solar cells and bulk n-type and p-type silicon material. The p on n silicon solar cells used in this experiment were commercial, off-the-shelf Hoffman 0.2 to 2.0 ohm-cm cells of nominal 9 per cent efficiency. These cells are from the same lot of cells that were used in the previous two high energy electron experiments and, hence, serve as a comparison with previous experiments. The n on p silicon solar cells were specially constructed devices in which base material resistivity was controlled and selected to within plus or minus 5 per cent for the reduction of data scattering due to variations about nominal resistivity. The resistivities were actually measured after the final diffusion prior to the application of contacts. The resistivities used for the n on p cells were 1.3, 3.3, and 10.6 ohm-cm. In addition, some 21 ohm-cm n on p silicon solar cells were tested at 1 Mev but were not available for the higher energy experiments. Several n on p 1.2 ohm-cm Western Electric cells from the same lot

used in the previous experiments were included in the experiments for comparison with previous data and also for comparison with the 1.3 ohm-cm n on p Hoffman solar cells.

In addition to the solar cells, 150 ohm-cm p-type and 100 ohm-cm n-type silicon were included. These specimens were pre-cut to the conventional six arm bridge configuration for post-irradiation measurements of Hall effects. These measurements of Hall effects, in addition to measurements of diffusion length versus temperature on the solar cell specimens, are analyzed to obtain information on the energy levels and defect mechanisms induced as a function of electron energy.

Measurements

A large number of measurements were performed on all specimens prior to, during, and after the irradiations. Some measurements were performed during the actual conduction of the irradiation at the linac site. Other measurements, such as minority carrier diffusion lengths and Hall effects, which could not be conducted at the linac site were performed at the STL laboratories immediately after completion of the irradiations. The complete series of measurements will be described in this section.

Minority carrier diffusion lengths were measured on each solar cell before and after irradiation. These measurements were obtained using the STL 1 Mev Van de Graaff. This technique for diffusion length measurement has been described in the literature[3] and consists of relating the observed steady state short circuit current produced with ionizing radiation to the minority carrier diffusion length of the bulk material. Minority carrier lifetime can be obtained from this measurement using the diffusion coefficient, D, of the carriers in the material of interest. With these diffusion length measurements, a commonly used damage constant, known as a K

value, is obtained with the following equation:

$$\frac{1}{L^2} = \frac{1}{L_o^2} + K\Phi \qquad (1)$$

which reduces to

$$K = \frac{1}{\Phi}\left(\frac{1}{L^2} - \frac{1}{L_o^2}\right) \qquad (2)$$

The principal requirement for this K value to be meaningful is that a log-log plot of diffusion length versus integrated flux exhibit a -1/2 slope. If this condition is not met, then different K values will be obtained on any given cell depending upon the integrated flux chosen to calculate the K value. Therefore, preliminary experiments are always conducted with the 1 Mev STL Van de Graaff on a given lot of cells before performing an off-site experiment to insure that the cells follow these characteristic degradation equations based on simple displacement theory.

Minority carrier diffusion lengths were also measured indirectly at the linac site through the established relation between short circuit current and minority carrier diffusion length for a given lot of cells. This relationship between short circuit current and minority carrier diffusion length is established for any given lot of cells with the 1 Mev Van de Graaff before proceeding to an off-the-site experiment. Minority carrier diffusion length values obtained with this indirect technique are then compared with minority carrier diffusion lengths measured directly after the completion of the experiments. In addition, all cells irradiated at the higher electron energies are checked for injection level dependence of the minority carrier diffusion length over a range extending from approximately one-sun illumination down to the limits imposed by minimum Van de Graaff beam currents and signal-to-noise levels. This injection level range covers approximately six orders of magnitude. Although

it is predicted by Hall, Shockley-Read recombination statistics that minority carrier lifetime, and hence minority carrier diffusion length, must exhibit injection level dependence, the injection level region in which this dependence occurs is important in the analysis of the data to insure that measurements made at different injection levels be comparable.

I-V characteristics were obtained on all solar cells with a 2800°K unfiltered tungsten illumination source. The approximate sunlight equivalent intensity of this illumination source is 110 to 130 mw/cm^2. Due to the differences between the spectral content of solar illumination and 2800°K tungsten illumination and the spectral differences in various types and manufacturers' solar cells, it is not possible to maintain constant absolute intensity on the light table and at the same time specify constant sunlight equivalent illumination. Therefore, this illumination source is absolutely calibrated and this calibration has been maintained over the last four years for purposes of comparing data on a large number of different experiments. As a result, the actual sunlight equivalent intensity will vary between different types of cells depending upon their initial diffusion lengths and surface characteristics. The choice of 2800°K tungsten illumination is based on its ease of reproducibility and maintenance over a long period of time and the fact that it amplifies the base region diffusion limited portion of the solar cell output which is most directly affected by charged particle irradiation, and minimizes differences due to variations in surface characteristics due to the lack of short wavelength energy in the tungsten spectrum. Although no solar illumination measurements were obtained on these cells, previous measurements obtained in a large number of experiments allow reasonable predictions of performance under solar illumination based on the tungsten illumination data.

From the I-V characteristics which are obtained after each individual radiation exposure, plots of short circuit current density, J_{sc}, versus integrated electron flux are obtained. These short circuit current densities are expressed in terms of ma/cm^2 for a 90 per cent active area device. Hence, devices with different grid structures than those of the standard device with a 1 mm wide collector strip running the long edge of the cell are normalized to this configuration. Once again, this normalization to a standard device is necessary in order to perform meaningful comparisons of data on different types of cells irradiated over the years in different experiments. For example, short circuit current density in terms of ma/cm^2 for a 1 x 2 cm cell with the collector strip located along the length of the cell would be obtained by simply dividing the observed short current by a factor of two, whereas short circuit current density for a cell with the collector strip located along the short edge would be obtained by dividing the observed short circuit current by a factor of 2.11. The I-V curves are also used to obtain degradations of open circuit voltage and maximum power output as a function of integrated flux.

In order to obtain a damage constant from the plots of short circuit current degradation versus integrated flux for comparison with K values and for determination of energy dependence, a value known as the critical flux is determined. Critical flux was defined several years ago as integrated flux required to reduce the short circuit current 25 per cent. This amounted to a reduction in short circuit current under $2800^{\circ}K$ tungsten illumination from 25 ma/cm^2 initial to 19 ma/cm^2 for a cell with a minority carrier diffusion length of 100 microns under an illumination of approximately 110 mw/cm^2 sunlight equivalent. During the past few years, however, typical minority carrier diffusion lengths have been observed to range from 175 microns to 225 microns. Since the normal condition is for the minority carrier diffusion lengths to degrade to equal values

independent of original values for a given resistivity and type of material, the definition of critical flux as integrated flux required to produce a short circuit current of 19 ma/cm^2 has been retained, even though it now represents more than 25 per cent degradation under tungsten illumination for current state-of-the-art solar cells. This approach allows meaningful comparison of data obtained on current state-of-the-art devices and data previously obtained over the past several years where original output characteristics were somewhat lower due to lower minority carrier diffusion lengths. Since K in Eq. (2) is inversely proportional to integrated flux, the reciprocal of the critical flux is plotted versus energy for comparison with K values. As in the case previously discussed with minority carrier diffusion length measurements, specimens from each individual lot of cells are irradiated with 1 Mev electrons prior to any off-the-site irradiations to insure that the slope of the short circuit current degradation characteristic follows the 6.25 ma/cm^2-decade slope characteristic of normal solar cells illuminated under these conditions.

After completion of the series of experiments at the linac site, further measurements were performed in the laboratory to delineate the energy levels responsible for the observed degradations. Hall effects measurements on the p-type and n-type specimens are performed on specimens irradiated at each energy at several integrated fluxes to determine the energy levels responsible for majority carrier trapping. In addition, minority carrier diffusion length versus temperature measurements are obtained using the Van de Graaff to illuminate a solar cell placed in a cryostat. From these data, dependence of minority carrier lifetime on temperature is obtained. This technique has the advantage over direct measurements of minority carrier lifetime with pulsed techniques in that the effects of trapping levels are removed due to the steady state conditions of the measurement as opposed to the conventional transient techniques

for measuring minority carrier lifetime. These data are then analyzed using Hall, Shockley-Read statistics in an effort to fit the observed slopes with the particular energy level responsible for minority carrier recombination.

Dosimetry

In order to obtain quantitative, accurate data, particular attention was given to measurements of beam energy, distribution, and intensity. Electron beam energy was determined by General Atomic personnel with a calibrated steering magnet. This magnet had been previously calibrated through a series of range energy relationships to within plus or minus 2 per cent. Magnet current was supplied by a regulated power supply insuring a constant magnetic field through the steering magnet. Any appreciable drift or change in beam energy due to operating characteristics of the accelerator would result in loss of beam at the port where the experimental apparatus was located. Corrections were applied for energy loss of the beam in traversing the exit port window and air in the determination of the energy incident upon the test specimens.

Beam spreading was accomplished with quadripole focusing magnets and air scattering to produce a beam spot large enough to accommodate the test specimens. Polaroid film was used to determine beam position and distribution over the beam area and to position the test specimens. The Polaroid film was used as a coarse indicator of beam distribution, and solar cell degradation as a function of position was used as a more accurate determination of beam distribution. The quadripole magnets were driven with regulated power supplies and found to be quite stable. Due to the small diameter of the accelerator drift tubes, however, there was a practical limit to the maximum beam spot size that could be produced in the drift tubes. To obtain further defocusing, the experimental apparatus was located a sufficient distance from the exit port window to take

advantage of small angle air scattering for further improvement in beam size and distribution. Particular distances between the experimental apparatus and the beam exit port window were determined by the energy of the beam and ranged from six inches to three feet. In all of the experiments the beam area exceeded 25 cm^2 at half of the peak intensity. Only the center 4 cm^2 of the total beam was used for sample irradiation wherein intensity gradients were less than 5 per cent.

Electron intensity was monitored with a Faraday cup of conventional design. The inner sensing chamber was constructed of copper 50 Mev thick and was mounted in a larger evacuated chamber which was fore pumped and trapped to a pressure of less than 10^{-3} Torr. The bottom or target area of the Faraday cup contained a 5 Mev thick aluminum plate to reduce the back-scattered electron component to a minimum. In addition, a copper back-scatter shield was utilized to reduce the back scatter solid angle a factor of ten. Additional back scatter control was exercised through the application of grid bias directly above the entrance aperture to the inner sensing chamber. Application of grid voltage from -400 to +400 volts indicated that the low energy back-scattered component had been reduced to less than 2 per cent and further that forward scattering from the 0.005 inch aluminum vacuum window of the Faraday cup was less than 1 per cent. Calculations of the high energy back-scatter component for the geometry and materials used here indicate an error of less than 1 per cent for this component. An estimate of the over-all accuracy of the Faraday cup is a maximum error of less than 5 per cent. Comparisons of beam current with apparatus utilized by General Atomic personnel were in agreement to within better than 3 per cent. The output of the Faraday cup was fed directly to an integrating amplifier system which measured both current and integrated charge to an accuracy of 1 per cent. This type of instrument is ideal for accepting high impedance inputs such as

Faraday cups since it presents essentially zero input impedance to the Faraday cup and eliminates errors due to leakage currents.

Experimental Techniques

The test specimens were mounted in the central 4 cm^2 area on thin aluminum plates. These plates in turn were placed in a jig indexed directly in front of the Faraday cup, and integrated flux measurements were obtained simultaneously with the irradiation of the test specimens. Each group of specimens was exposed to a predetermined integrated flux and removed for post-irradiation measurements, then re-inserted in the beam for further irradiations. When a sufficient number of irradiations had been performed to define a straight line function of the degradation of the short circuit current with the logarithm of the integrated flux, the specimens were removed and stored for later post-irradiation measurements. A minimum of four specimens of each individual type was tested at each energy in an alternating sequence such that if serious accelerator or equipment changes occurred, the data would exhibit corresponding deviations. In the event deviations or unexpected behavior occurred, machine characteristics would be examined and, if necessary, an adequate number of additional cells would be tested to determine if the deviation were machine-produced or were caused by deviations in the test specimens themselves, such as deviations in resistivity.

Beam alignment and distribution were continuously checked throughout each series of experiments at any given energy by Polaroid film. In addition, beam energy measurements were performed utilizing the calibrated steering magnet before and after each series of runs to determine any deviation of beam energy throughout any given series of irradiations.

Pre-irradiation Experiments

As mentioned in previous sections, a complete series of 1 Mev electron radiation degradations were performed on sample cells from each lot of cells prepared for the high energy experiments. The purpose of these irradiations was twofold: (1) to acquire degradation characteristics in the energy range from 0.4 to 1.0 Mev for each particular group of cells and (2) to qualify the groups of cells as to linearity and slope of both the short circuit current and minority carrier diffusion length degradation characteristics. The experimental conditions utilized on the 1 Mev STL Van de Graaff experiment are much simpler than those required at the higher energies and further are described in detail elsewhere[4]. In essence, the accuracy with which beam energy, distribution, and intensity can be determined with this machine is better than plus or minus 2 per cent. For these reasons and also because of the ready availability of this machine for further calibrations and checks as required, all data are normalized and analyzed to 1 Mev data where necessary or desirable.

III. EXPERIMENTAL RESULTS

Separate linac experiments were conducted at four energies: 40.0 Mev, 16.4 Mev, 6.4 Mev, and 2.7 Mev. Included with these data and experimental results are additional data obtained on the STL Van de Graaff at 1.0 Mev, 0.6 Mev, and 0.4 Mev. The resulting electron energy dependence of the radiation damage is determined by utilizing both K values and reciprocal critical fluxes. The K values were obtained from diffusion length measurements with the Van de Graaff accelerator and with the calibrated light source. The reciprocal critical flux determinations were acquired from short circuit current degradation characteristics. In addition, several energy levels were obtained from both resistivity dependence of the radiation damage and Hall effects measurements on bulk silicon.

Additional measurements of minority carrier diffusion length dependence on temperature are currently underway, but these experiments and the subsequent data analysis are not completed at the time of the writing of this paper and, therefore, are not included here but will be considered in detail in future reports. The remainder of this section will be devoted to the presentation of the experimental data and the results of the subsequent data analysis.

Degradation of Solar Cell Output Characteristics

The inclusion of all the raw data obtained in this series of experiments is beyond the scope of this paper; however, these data will be presented in a later NASA report, Contract NAS5-3805, under which this work was sponsored. Typical data plots will be included, however, to illustrate the type of data obtained and the techniques utilized in their analysis. The final results of the analyses of these data are summarized in Table I. Included in Table I are the values of critical flux, reciprocal critical fluxes, and K values for each cell type at each energy studied. It is from these data that subsequent plots of damage coefficients versus energy were obtained.

Shown in Figure 1 are typical diffusion length degradation curves as a function of electron integrated flux at 1.0 Mev for several types of cells. It should be noted that the data points fit the -1/2 slope, shown as a solid line, quite accurately resulting in a meaningful K value in the qualification of these cells to simple displacement theory as given by Eqs. (1) and (2) in the previous section. Figure 2 presents a typical I-V characteristic versus integrated electron flux at 16.4 Mev. This figure is typical of the actual raw data obtained at the linac site and is the source of subsequent plots of short circuit current density (J_{sc}), open circuit voltage (V_{oc}), and maximum

TABLE I

Φ_c and K Values as a Function of Energy of Solar Cell Type

	Φ_c (Electrons/cm^2)	Φ_c^{-1} (cm^2/Electron)	K (Electrons^{-1})	E (Mev)
CEG	4.90×10^{13}	2.04×10^{-14}	2.00×10^{-9}	0.4
OUMX	1.75×10^{15}	5.70×10^{-16}	7.35×10^{-11}	
OUMY	2.43×10^{15}	4.20×10^{-16}	5.50×10^{-11}	0.6
OUOX	4.55×10^{15}	2.20×10^{-16}	3.30×10^{-11}	
CEG	9.25×10^{12}	1.08×10^{-13}	8.00×10^{-9}	
OUMX	6.00×10^{14}	1.67×10^{-15}	2.50×10^{-10}	
OUMY	9.60×10^{14}	1.04×10^{-15}	1.48×10^{-10}	1.0
OUOX	1.90×10^{15}	5.30×10^{-16}	8.33×10^{-11}	
OUOY	2.90×10^{15}	3.50×10^{-16}	5.30×10^{-11}	
CEG	4.35×10^{12}	2.30×10^{-13}	1.77×10^{-8}	
OUMX	1.54×10^{14}	6.50×10^{-15}	1.17×10^{-9}	
OUMY	2.27×10^{14}	4.40×10^{-15}	7.80×10^{-9}	2.7
OUOX	4.32×10^{14}	2.30×10^{-15}	4.45×10^{-10}	
CEG	2.90×10^{12}	3.45×10^{-13}	3.11×10^{-8}	
OUMX	5.90×10^{13}	1.70×10^{-14}	2.62×10^{-9}	
OUMY	9.00×10^{13}	1.11×10^{-14}	1.72×10^{-9}	6.4
OUOX	1.80×10^{14}	5.55×10^{-15}	9.92×10^{-10}	
CEG	2.65×10^{12}	3.80×10^{-13}	3.70×10^{-8}	
OUMX	2.85×10^{13}	3.50×10^{-14}	4.15×10^{-9}	
OUMY	4.55×10^{13}	2.20×10^{-14}	3.47×10^{-9}	16.4
OUOX	9.10×10^{13}	1.10×10^{-14}	1.84×10^{-9}	
MWM	1.28×10^{13}	7.80×10^{-14}	5.04×10^{-9}	
CEG	2.38×10^{12}	4.20×10^{-13}	4.15×10^{-8}	
OUMX	2.10×10^{13}	4.75×10^{-14}	8.30×10^{-9}	
OUMY	3.08×10^{13}	3.15×10^{-14}	5.61×10^{-9}	40.0
OUOX	6.00×10^{13}	1.67×10^{-14}	2.79×10^{-9}	

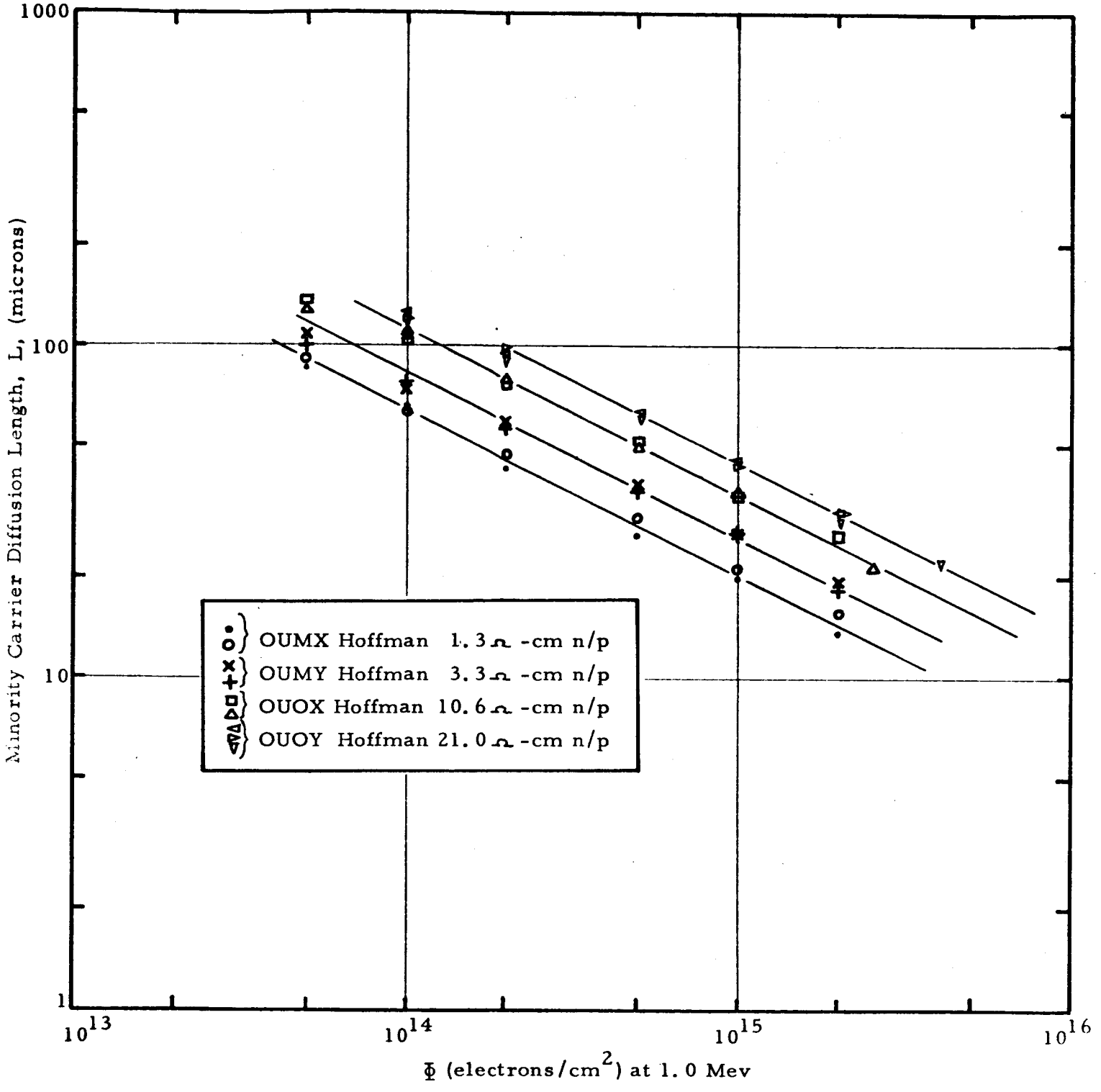

Figure 1. TYPICAL MINORITY CARRIER DIFFUSION LENGTH DEGRADATION DATA

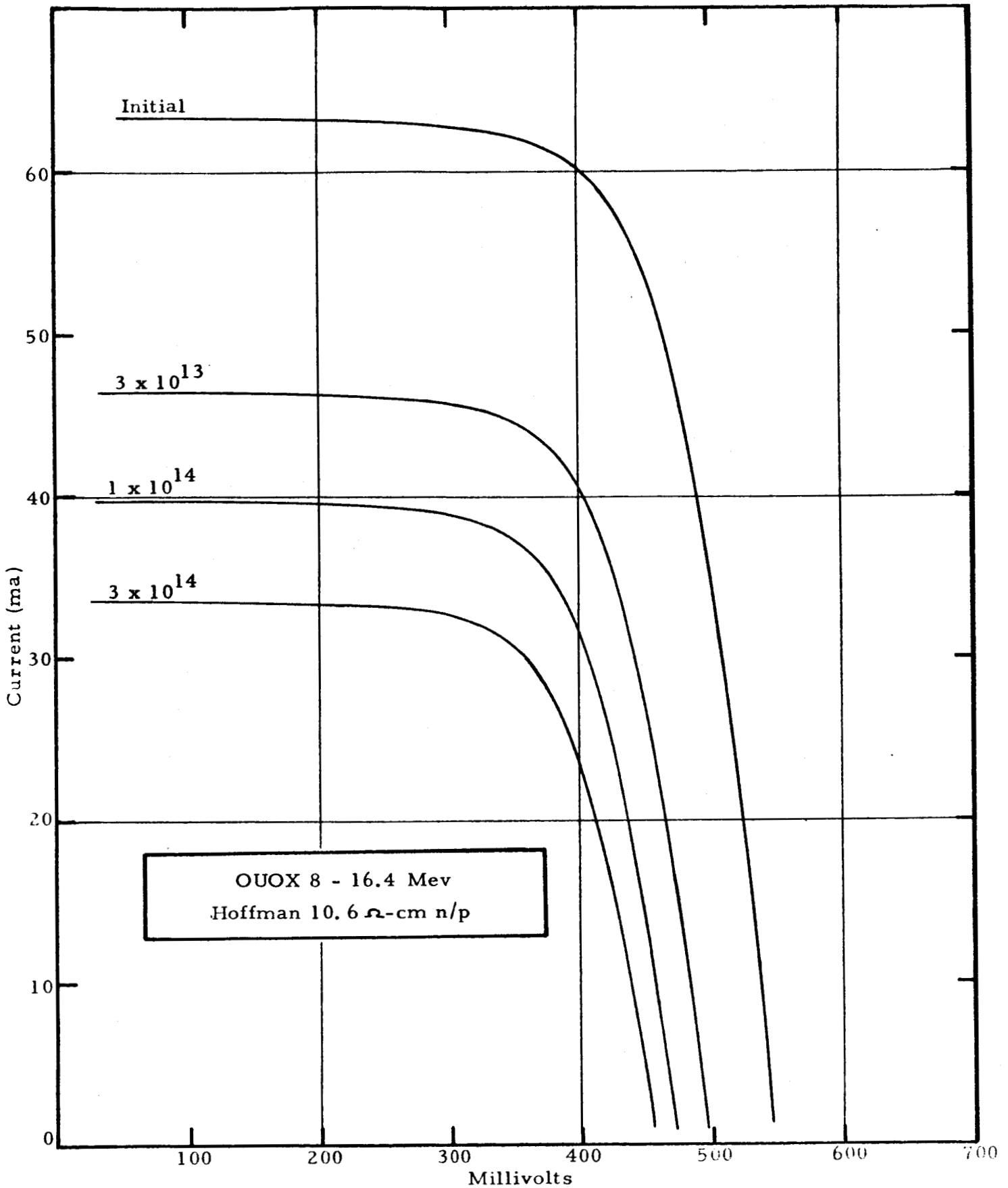

Figure 2. TYPICAL I-V CHARACTERISTIC DEGRADATION DATA

power output (P_{max}) versus integrated electron flux. Shown in Figure 3 is a typical plot of J_{sc} degradation versus integrated flux for cells irradiated with 2.7 Mev electrons. Note that a minimum of four cells and sometimes six cells of each given type are shown on the curve. The scatter among each individual group of cells is typically less than plus or minus 2 per cent. A standard slope of 6.25 ma/cm^2-decade fits all the data quite well. The degradation slope under equivalent sun illumination would be approximately 4.5 ma/cm^2-decade for 1 x 2 cm^2 cells having an active area of 1.8 cm^2. The Φ_c values shown in Table I are the integrated fluxes required to produce a J_{sc} of 19 ma/cm^2 on plots of this type. A shift in cell type or energy simply represents a lateral shift of the characteristic slope as shown in Figure 3 to the appropriate Φ_c value indicated in Table I. The initial J_{sc} values for these cells lie in the 27 to 29 ma/cm^2 range with corresponding initial minority carrier diffusion lengths in the 175 to 225 micron range.

Shown in Figure 4 and Figure 5 are plots of K versus E and Φ_c^{-1} versus E for the p on n cells tested in this series of experiments. Also shown in these figures are some data obtained in a previous series of experiments. The solid line shown in Figure 4 is identical to the solid line shown in Figure 5 and is determined by a best fit to both the K values and the Φ_c^{-1} values, jointly. The dashed line shown in Figures 4 and 5 represents predictions based on classical Coulomb scattering and simple displacement theory. As is observed, the fit of the experimental data with the predicted energy dependence is reasonably good. It is interesting to note that the high energy tail observed in previous experiments is not evidenced here and was, therefore, most probably due to data scattering through resistivity variances or undetected shift in machine characteristics in the previous experiment.

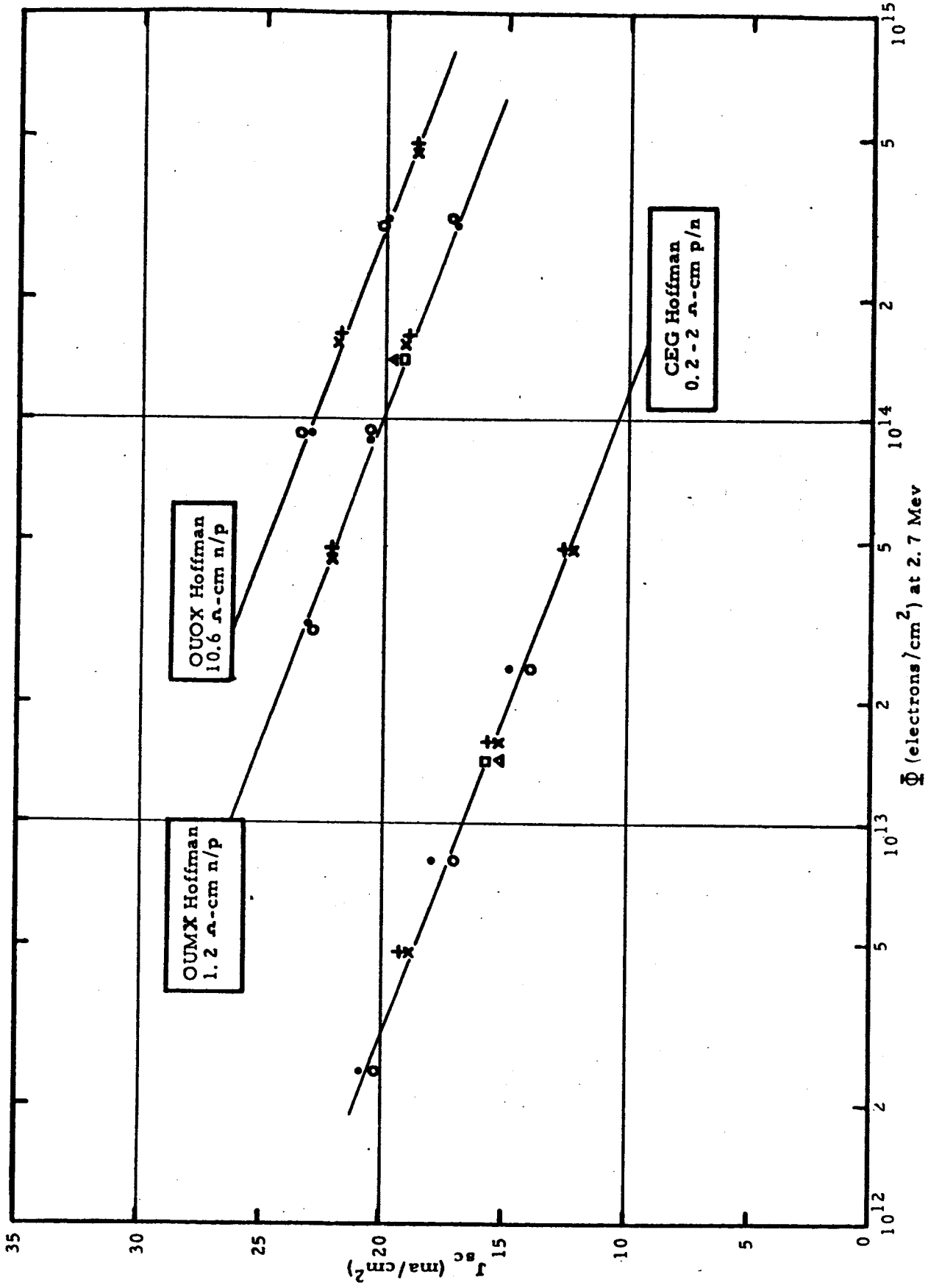
OUOX Hoffman
10.6 Ω-cm n/p
OUMX Hoffman
1.2 Ω-cm n/p
CEG Hoffman
0.2 - 2 Ω-cm p/n
J_{sc} (ma/cm^2)
Φ (electrons/cm^2) at 2.7 Mev
35
30
25
20
15
10
5
0
10^{12}
2
5
10^{13}
2
5
10^{14}
2
5
10^{15}

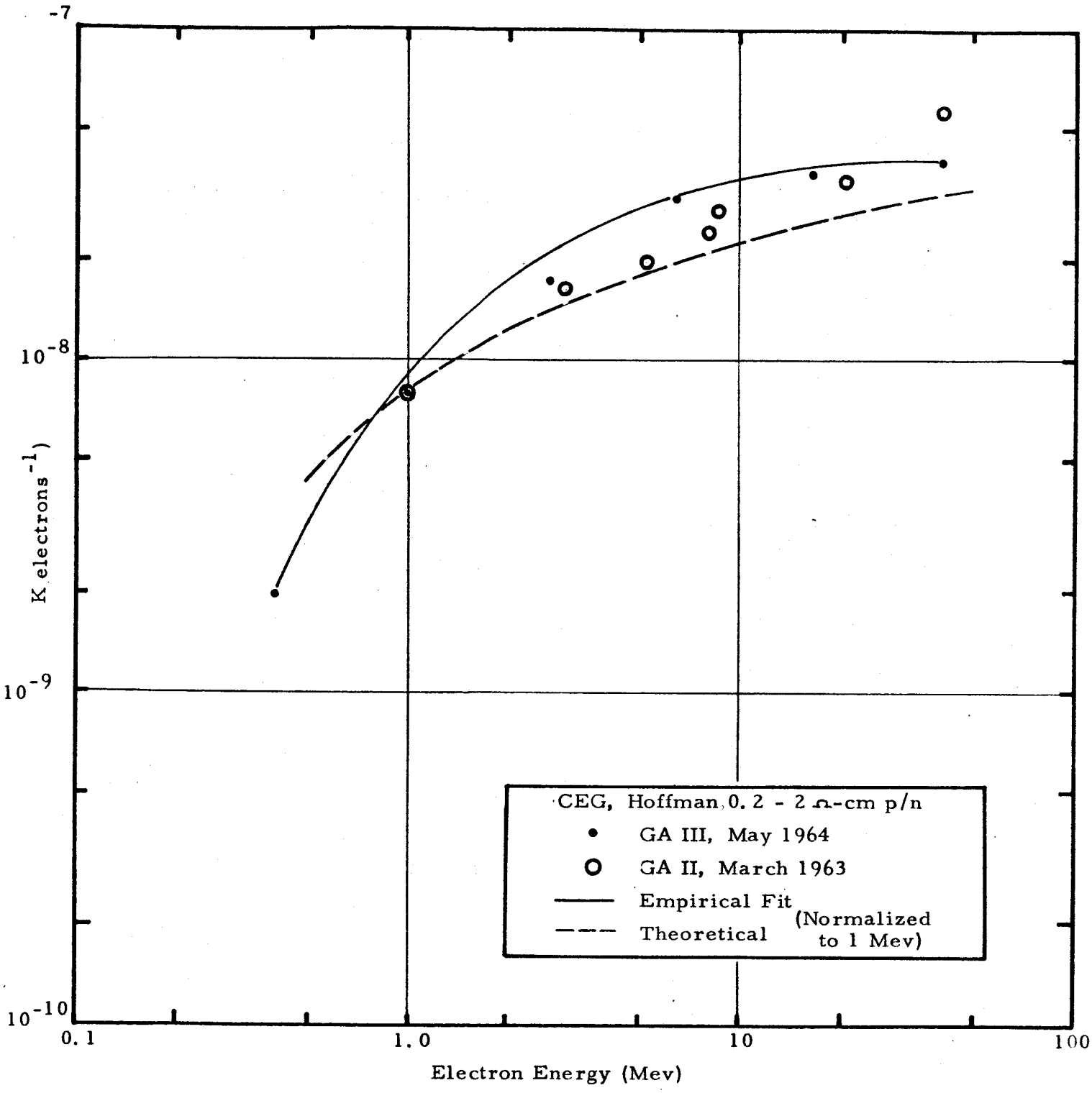

Figure 4. ELECTRON ENERGY DEPENDENCE OF K VALUES FOR P ON N SILICON SOLAR CELLS

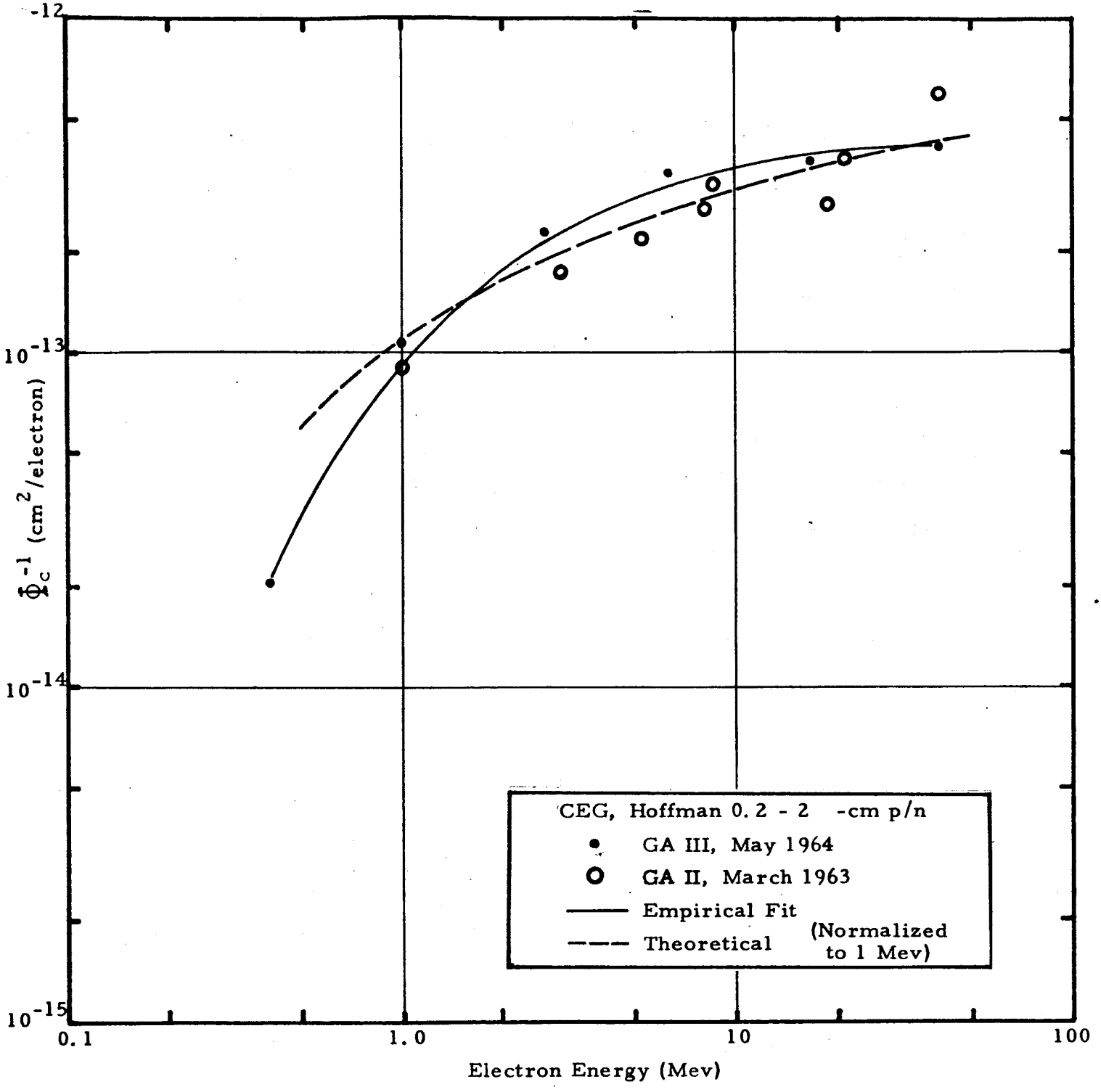

Figure 5. ELECTRON ENERGY DEPENDENCE OF Φ_c^{-1} VALUES FOR P ON N SILICON SOLAR CELLS

Figures 6 and 7 show the energy dependence of the K values and the Φ_c^{-1} values for the n on p silicon solar cells tested. The solid lines drawn through the data points are identical in both figures in shape as well as separation. The good fit of the sets of lines to the data indicates agreement in the energy dependence as obtained by K values with that obtained by Φ_c^{-1} values. Further, each line in the set of lines is parallel to each other, indicating that the energy dependence of the degradation of silicon solar cell characteristics is independent of base material resistivity in this energy range. Shown in both Figures 6 and 7 at 16.4 Mev are data on the older Western Electric cells of the type used in previous experiments. These cells have a resistivity of 1.2 ohm-cm, and therefore are comparable with the 1.3 ohm-cm Hoffman cells. The K values indicate essentially identical values confirming that reproducibility is obtainable with materials from different sources processed at different times by different manufacturers. The agreement is not quite as good in Figure 7 on the basis of Φ_c^{-1} values, but this is anticipated on the basis that manufacturing techniques are continuously improving surface characteristics and over-all collection efficiencies which in turn affect the Φ_c^{-1} values. The dashed curve shown in Figures 6 and 7 indicates the predicted energy dependence based on relativistic Coulomb scattering and simple displacement theory. As evidenced in previous experiments, n on p cells and, hence, p-type silicon depart radically from this relationship since damage rates at 40.0 Mev are approximately a factor of 30 greater than those observed at 1.0 Mev as opposed to a factor of three as predicted by theory.

In all the K values presented in the previous figures, measurements of the dependence of the minority carrier diffusion length on injection level were performed. No injection level dependences of consequence were observed in the carrier density

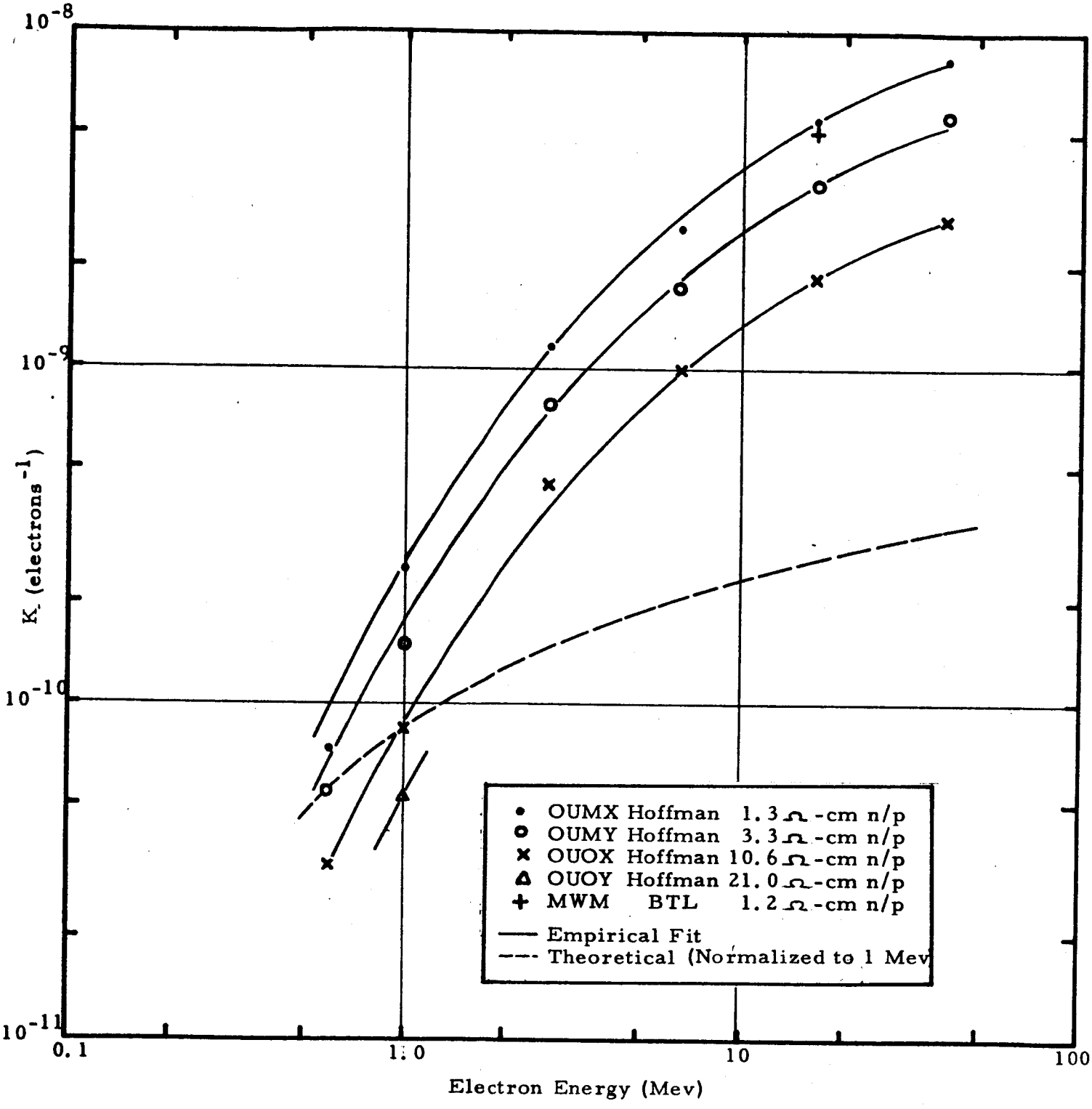

Figure 6. ELECTRON ENERGY DEPENDENCE OF K VALUES FOR N ON P SILICON SOLAR CELLS

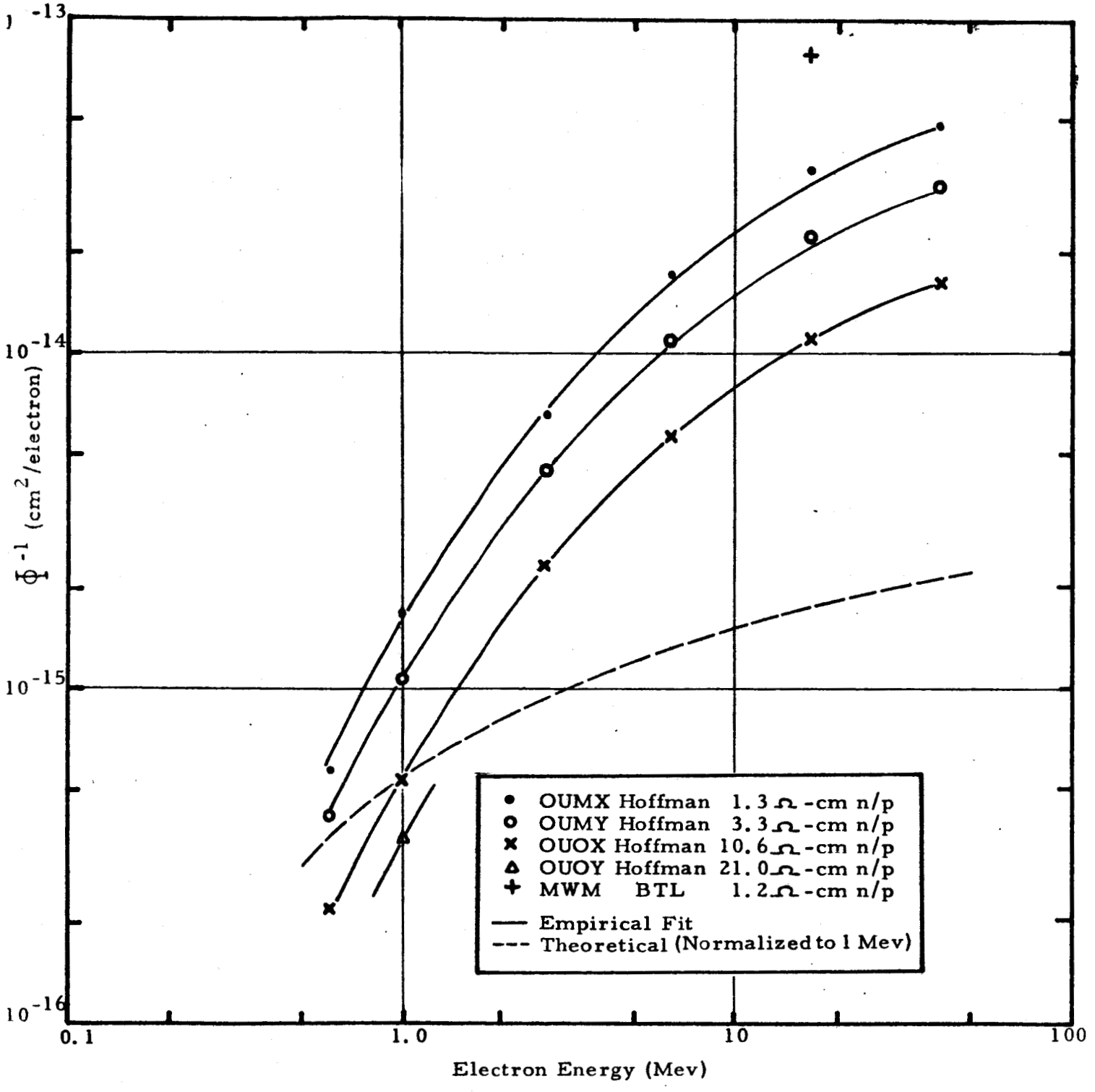

Figure 7. ELECTRON ENERGY DEPENDENCE OF Φ_c^{-1} VALUES FOR N ON P SILICON SOLAR CELLS

range covered in these experiments, i.e., from one sun illumination level to approximately 10^{-6} sun illumination level. It is anticipated, however, that measurements at higher injection levels would indeed indicate injection level dependences as predicted by Hall, Shockley-Read recombination theory; however, the geometry and characteristics of these solar cells are such that appreciably higher injection levels cannot readily be obtained.

The typically observed degradation in V_{oc} as a function of integrated electron flux, material type, and resistivity is shown in Figure 8. Data scatter of approximately 5 to 10 mv is inherent in these data since solar cell cooling is provided by blowing ambient laboratory air over the specimens, and the temperature of the ambient air routinely varies $4^{o}C$ to $5^{o}C$, depending upon ambient heat loads and time of day. The observed degradation fits a straight line with a slope of approximately 40 mv/decade reasonably well in all cases regardless of cell type and resistivity. This degradation rate is considerably in excess of that observed by simply lowering the illumination level an amount corresponding to short circuit current degradation or sliding the original I-V characteristics downward on the current axis to the appropriate short circuit current value. The observed additional degradation in V_{oc} is most likely due to radiation-induced changes in the saturation current I_o and possibly the constant, A, which appears in the exponent of the diode equation. The initial values of V_{oc} and subsequent absolute values of V_{oc} as a function of integrated flux show the anticipated decrease with increasing resistivity. Not observed here, however, are increases in the degradation rate for the higher resistivity material. Actually, this lack of increased degradation rate for the higher resistivities is not surprising at the exposure levels used for these experiments. For example, an exposure of approximately 2×10^{15}

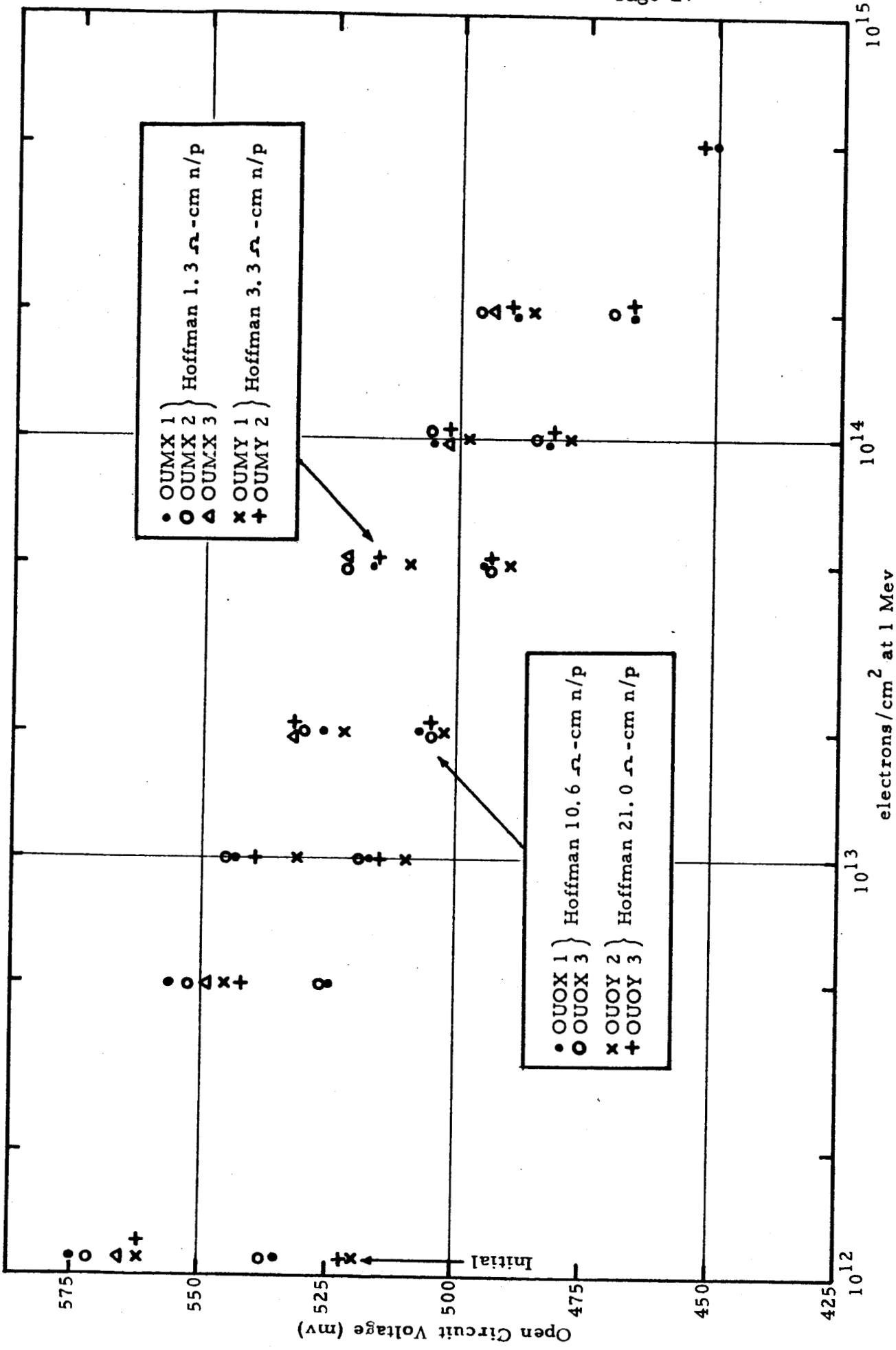

Figure 8. DEGRADATION OF OPEN CIRCUIT VOLTAGE AS A FUNCTION OF RESISTIVITY

e/cm^2 at 1.0 Mev would be required to introduce active defect concentrations equal to 10 per cent of the original majority carrier concentration in 20 ohm-cm p-type silicon. Since defect concentrations of this magnitude or greater would be required to produce resistivity increases, and hence additional open circuit voltage degradations, the absence of this effect in Figure 8 is expected. Additional exposures beyond 2×10^{15} e/cm^2 should result in an increase in V_{oc} degradation rates for the higher resistivity cells but adequate beam time for these longer exposures was not available in this series of experiments.

Figure 9 illustrates the effect of resistivity on maximum power output degradation as a function of integrated flux for a random selection of I-V characteristics. These data were obtained by correcting the appropriate I-V characteristics to equivalent 1.0 Mev integrated fluxes under solar illumination of approximately one sun intensity using a short circuit current degradation rate of 4.5 ma/cm^2-decade as determined by previous experiments[4]. As observed in Figure 9, the maximum power output degradation as a function of integrated flux is noticeably improved at higher resistivities even though the decreased voltages obtained at higher resistivities detracts from the increased radiation resistance of the short circuit current. The large amount of scatter evident in these data is due to the random selection of points and is indicative of what may be anticipated in the actual design of solar cell arrays using large numbers of commercially available solar cells.

Radiation Induced Energy Levels in Silicon

The Hall, Shockley-Read recombination statistics predict, for a given concentration of single recombination centers, the dependence of minority carrier lifetime on base material resistivity. Using experimental minority carrier diffusion lengths

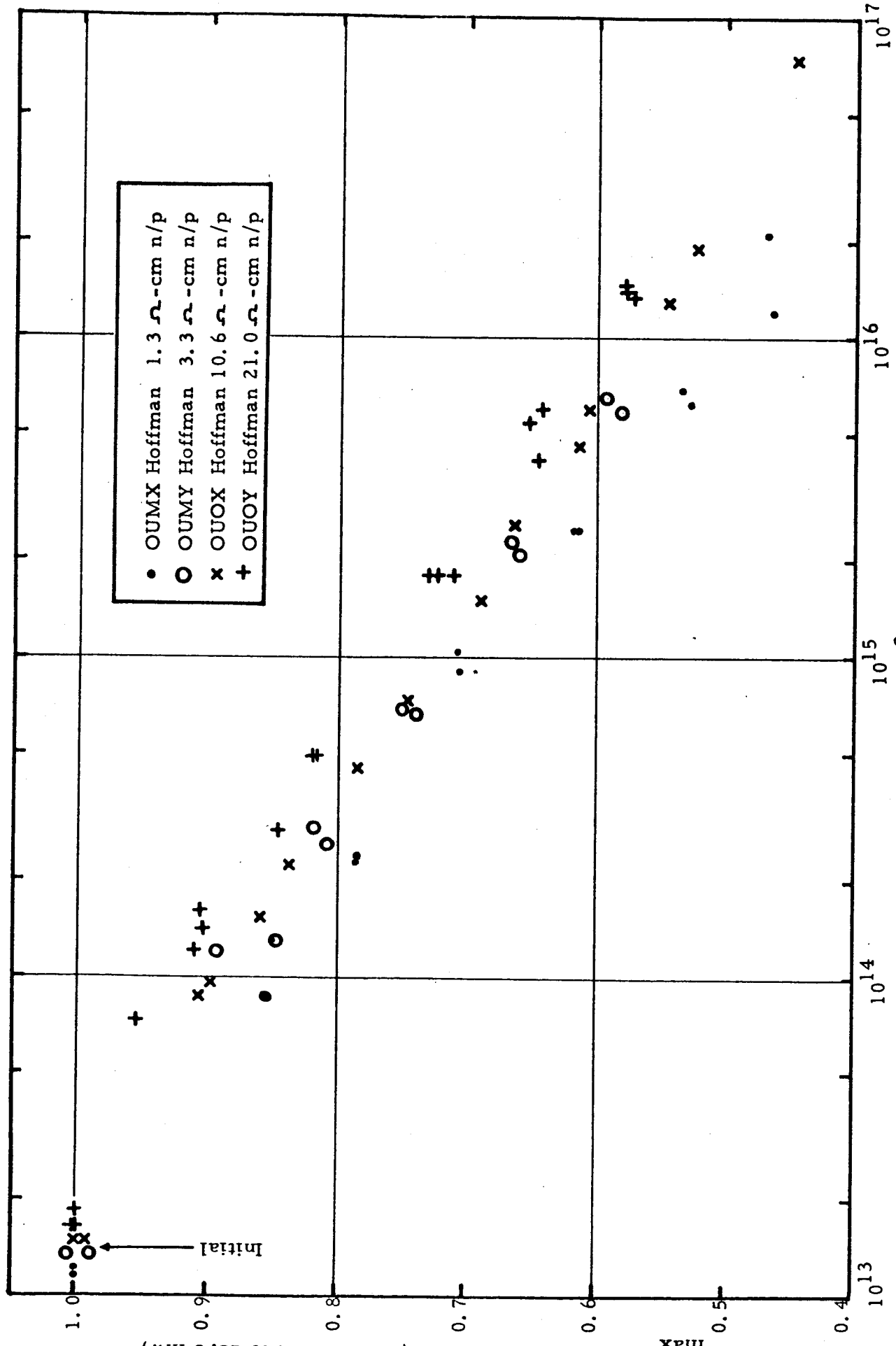

Figure 9. DEGRADATION OF MAXIMUM POWER UNDER SOLAR ILLUMINATION AS A FUNCTION OF RESISTIVITY

found in degraded cells with appropriate diffusion constants, carrier lifetimes can be calculated. In Figure 10 these lifetimes and the base resistivity of the degraded n on p-type cells are fitted to the theoretical curve for an energy level E_c - 0.17 ev. The cells examined had base resistivities of 1.3, 3.3, 10.6, and 21.1 ohm-cm. The experimental lifetime values are in good agreement with the theoretical predictions. The recombination center appears to be an acceptor, since τ_{no} is much larger than τ_{po}. Considerable evidence of this level has been reported by Hall effect measurements and recombination studies[5]. The level, also referred to as the Si-A center, has been identified by ESR studies[7]. It is thought to be a vacancy-oxygen pair. These results agree with those of Wertheim[5] in regard to the E_c - 0.17 ev level controlling recombination in electron irradiated p-type silicon, but differ from the results of Baiker[6]. Baiker concluded that electron irradiation of p-type silicon introduced donor type recombination center 0.18 ev above the valence band. Using the defect introduction rate of this level as determined by Hall measurements, n-type silicon, an electron capture cross section of approximately 10^{-15} cm^2, is obtained which is also in agreement with Wertheim's[5] data. Since the ratio of diffusion lengths of electron irradiated n on p cells of varying resistivity does not change with electron energy, the 0.17 ev level appears to control recombination for all electron energies considered.

Diffusion length measurements were also made as a function of temperature. A special vacuum dewar was constructed for this purpose. Minority carrier lifetimes were calculated from the following equations using published values for electron mobility.

$$D = \frac{\mu k T}{e}$$

$$\tau = \frac{L^2}{D}$$

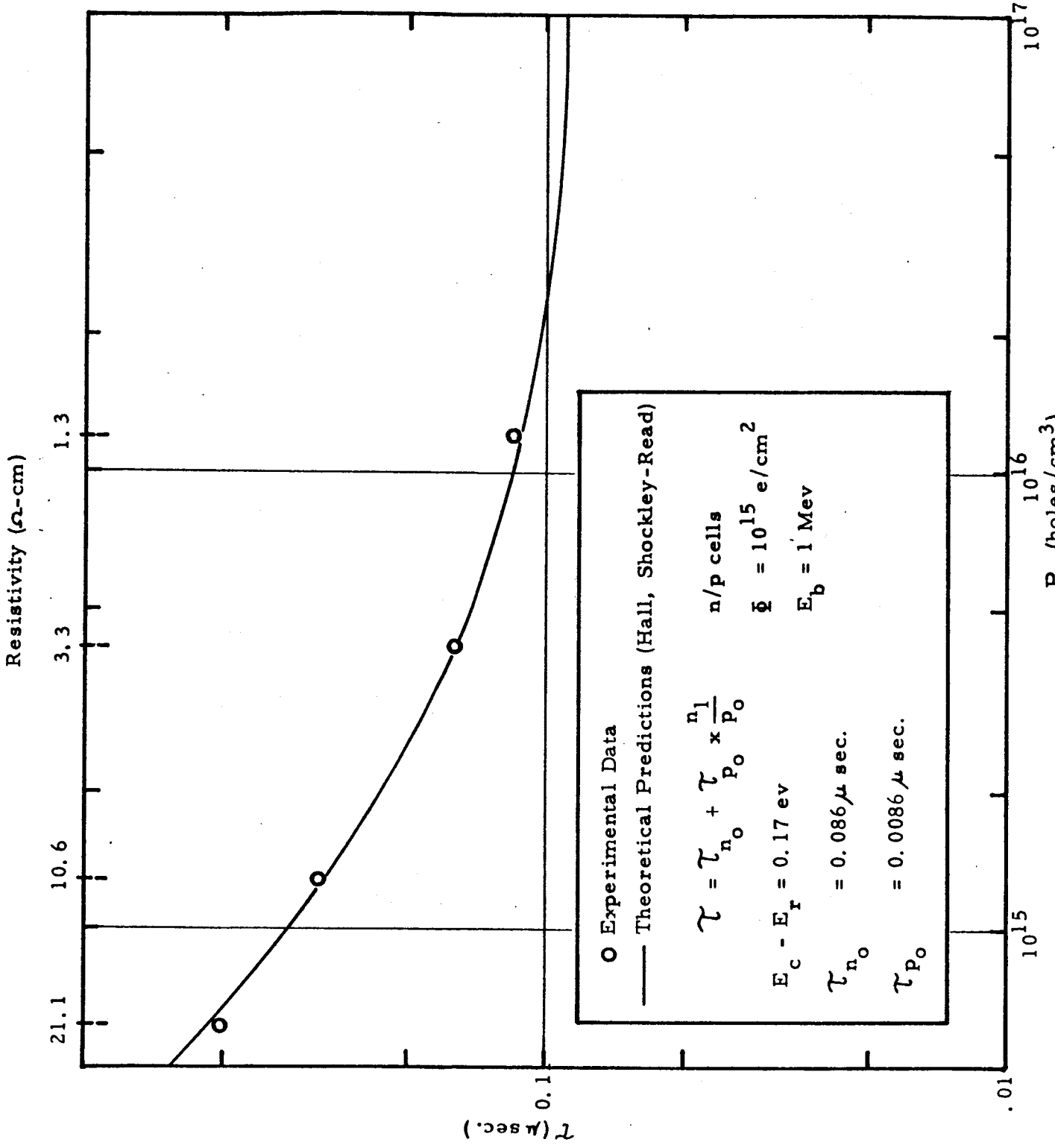

Figure 10. DEPENDENCE OF MINORITY CARRIER LIFETIME DEGRADATION ON RESISTIVITY

These lifetime values were compared to Hall, Shockley-Read theory. In Figure 11 the lifetime is plotted versus reciprocal temperature for n on p,21.1 ohm-cm irradiated solar cell. The slope of the points in the high temperature region indicates an activation energy of 0.17 ev. Two solid lines also shown on the Figure represent the theoretical variation of lifetime for a recombination center 0.17 ev below the conduction band and one 0.17 ev above the valence band. It is necessary to consider the temperature variation of the density of states for these calculations. The fit for E_c - 0.17 ev is good except at the lowest temperatures. The poor fit at low temperatures is probably due to lack of accurate diffusion constants for this range. Figure 12 shows identical data for n on p, 10 ohm-cm solar cell. Again, the experimental points fit the curve for a E_c - 0.17 ev recombination center. Since τ_{no} is much larger than τ_{po} in all cases, the recombination center appears to be an acceptor.

The type of analysis applied in Figure 10 assumes that the concentration of recombination centers depends only on the total electron flux and is independent of the dopants or resistivity. From the following Shockley-Read equations

$$\tau_{no} = \frac{1}{N_r \sigma_n \nu_t} \qquad \tau_{po} = \frac{1}{N_r \sigma_p \nu_t}$$

indicate that τ_{no} and τ_{po} are inversely proportional to the concentration of recombination centers. Since all samples studies in Figure 10, 11, and 12, were irradiated with 10^{15} e/cm^2, the determined values of τ_{no} and τ_{po} should not differ. The values found in these analyses differ by as much as a factor of two. This may be due to inaccuracies in the low temperature values of the diffusion constant. If this variation of τ_{no} is real, it would indicate a more complex relationship

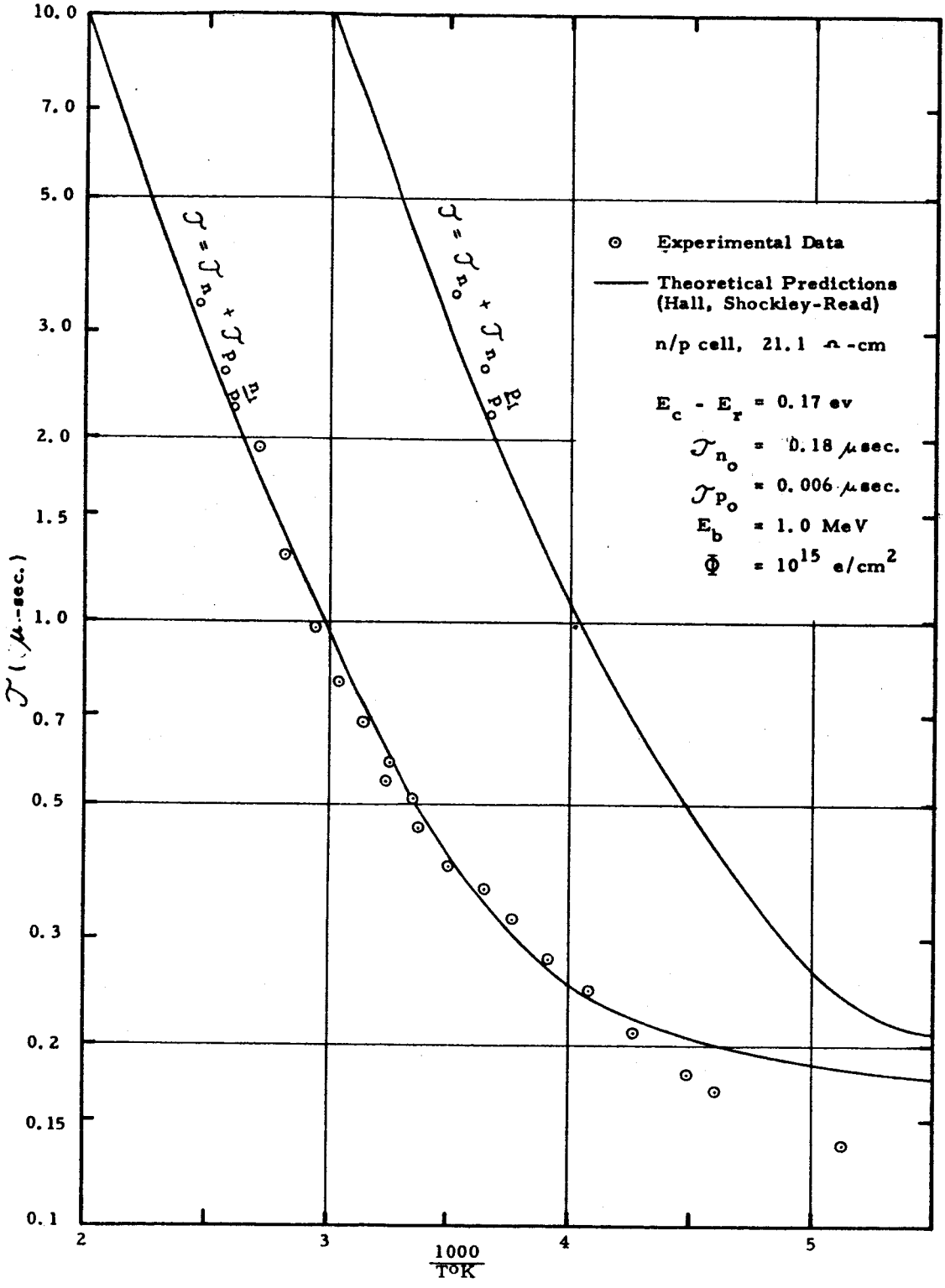

Figure 11. Dependence of Lifetime on Reciprocal Temperature

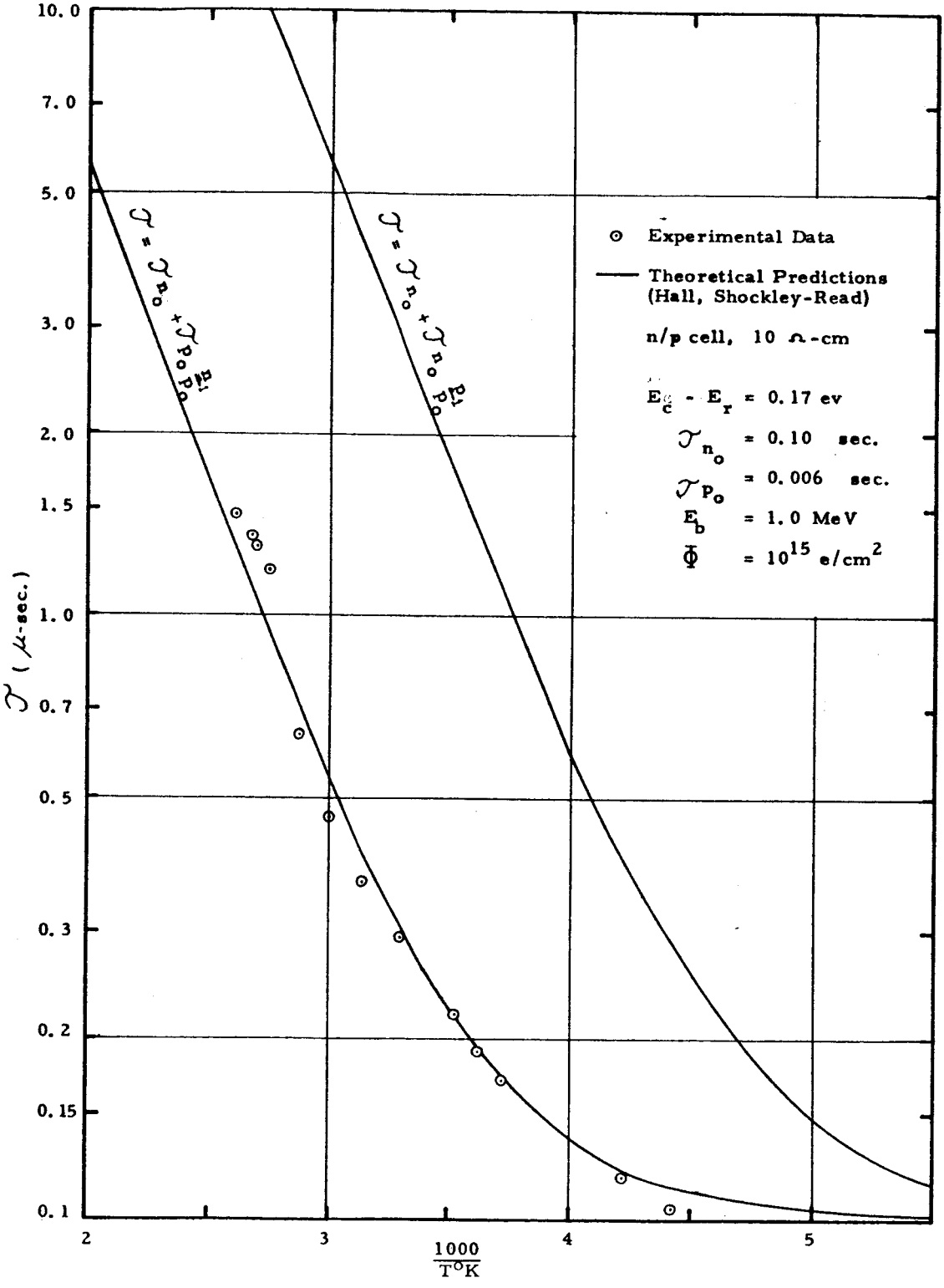

Figure 12. Dependence of Lifetime on Reciprocal Temperature

between defect production and resistivity. These variations in τ_{no} are relatively small compared to those reported by Baiker[9] for similar bombardments. Further work is planned to clarify these results.

This experiment has been complicated by annealing effects. Solar cells heated above 100°C, often have increased diffusion lengths after return to room temperature. This annealing voids the diffusion length data taken at higher temperatures. The effect is not found in recently bombarded cells. The temperature range of the annealing changes observed is not consistent with annealing studies reported by Bemski and Augustyniak[10]. This low temperature annealing in n on p cells will be studied further to clarify the annealing kinetics and the nature of the defects.

Studies of Hall coefficient changes after irradiation were made to supplement solar cell data. Samples of n and p-type crucible grown silicon were bombarded with electrons of various energies up to 40 Mev. The electron fluxes were controlled to allow detection of prominent energy levels and measurement of the introduction rate of these levels by techniques described by Wertheim[5]. The only level detected in the irradiated 150 ohm-cm p-type silicon was the E_v + 0.3 ev level[5,7]. In Figure 13, the introduction rate of this defect level is plotted as a function of electron energy. The data shown in the figure indicate that the defect introduction rate is a factor of 10 higher at 40 Mev over that at 1 Mev. Predictions for displacement theory indicate a factor of three increase. The experimental data also disagree with the observed factor of 30 increase found from K and Φ_c^{-1} values for n on p solar cells. Two energy levels were detected in the irradiated 100 ohm-cm n-type silicon. The levels E_c - 0.17 ev and the E_c - 0.4 ev were detected after irradiation with 2.7 to 39 Mev electrons. Both levels were reported by Hill[9]

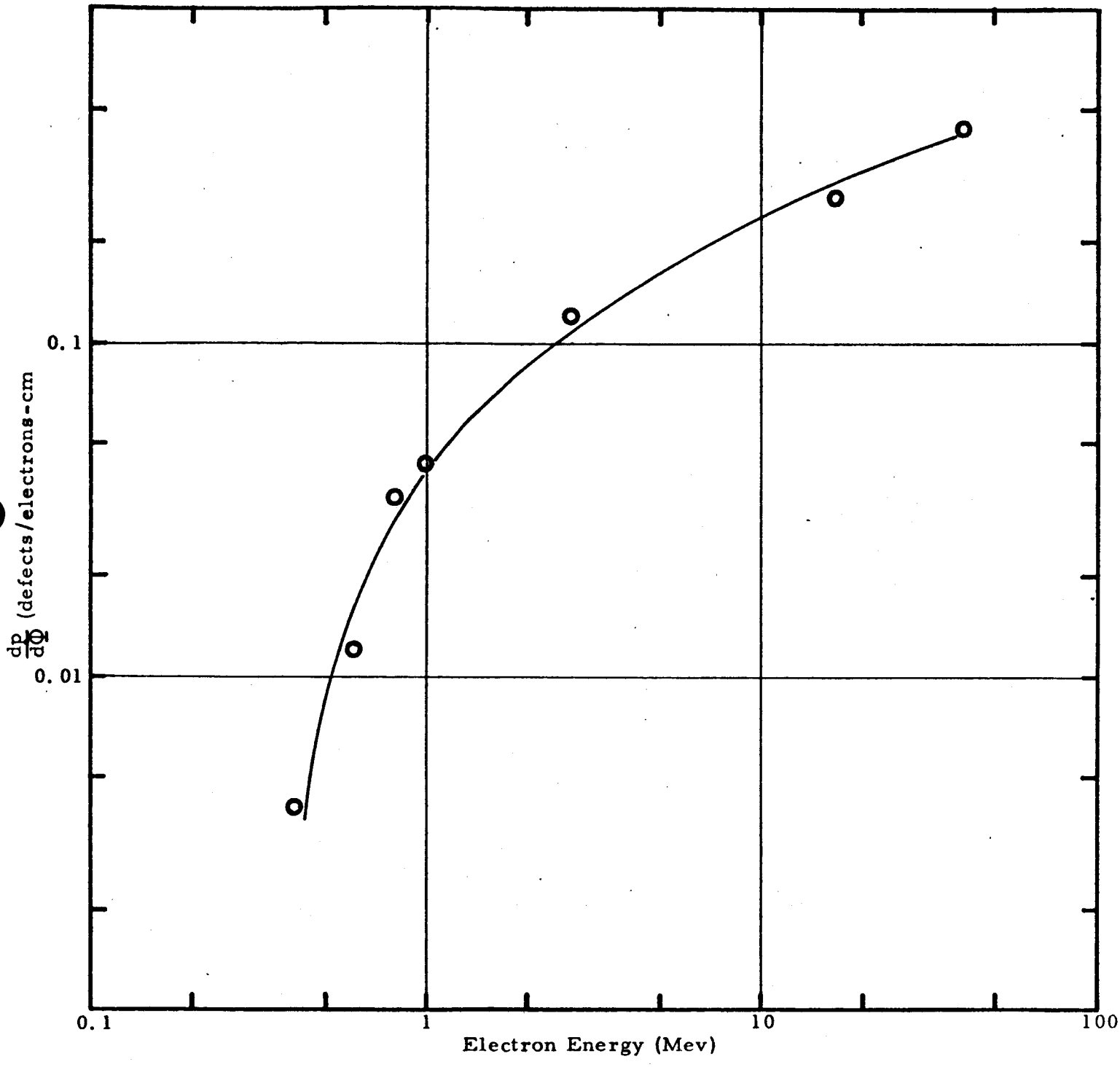

Figure 13. ELECTRON ENERGY DEPENDENCE OF THE $E_t - E_v = 0.3$ ev DEFECT LEVEL IN 150 OHM-CM P-TYPE SILICON

and are referred to as the Si-A and Si-E centers in ESR studies[7]. The 0.17 ev level is believed to be a vacancy-oxygen pair, and the 0.4 ev level is believed to be a vacancy-phosphorus pair. In Figure 14 the defect introduction rate for the 0.17 ev level is plotted as a function of electron energy. This introduction rate appears to be approximately constant at about 0.3 defects/electron-cm above 1 Mev. This is in contrast to the theory which predicts an increase of 3 from 1 Mev to 40 Mev. In summary, the data on energy levels are conflicting. The data for K and Φ_c^{-1} values for n-type cells are in good agreement with displacement theory energy variation. Neither the data for the 0.17 ev nor the 0.3 ev levels agree well with this theory, although the 0.17 data are in very rough agreement. This would imply that the 0.17 ev level may control degradation in n-type cells, but not in p-type cells. The Hall, Shockley-Read analysis of degradation in p-type cells indicates that the 0.17 ev level controls degradation. The data on introduction rate of the 0.3 ev level has some similarities to the K and Φ_c^{-1} data for p-type cells. Both curves rise much faster than single displacement theory, although not at identical rates. This may imply that the introduction of the 0.3 ev level is responsible for degradation of p-type cells. Additional study is required to clarify the data in regard to the conflicting conclusions.

IV. SUMMARY AND CONCLUSIONS

The primary objectives of this series of experiments were: (1) to obtain statistically significant and accurate quantitative data on the energy dependence of electron radiation damage in silicon, (2) to determine the effect of resistivity on the damage rate and energy dependence, and (3) to obtain data on the energy levels and defect mechanisms responsible for electron radiation damage in silicon. The first two objectives were

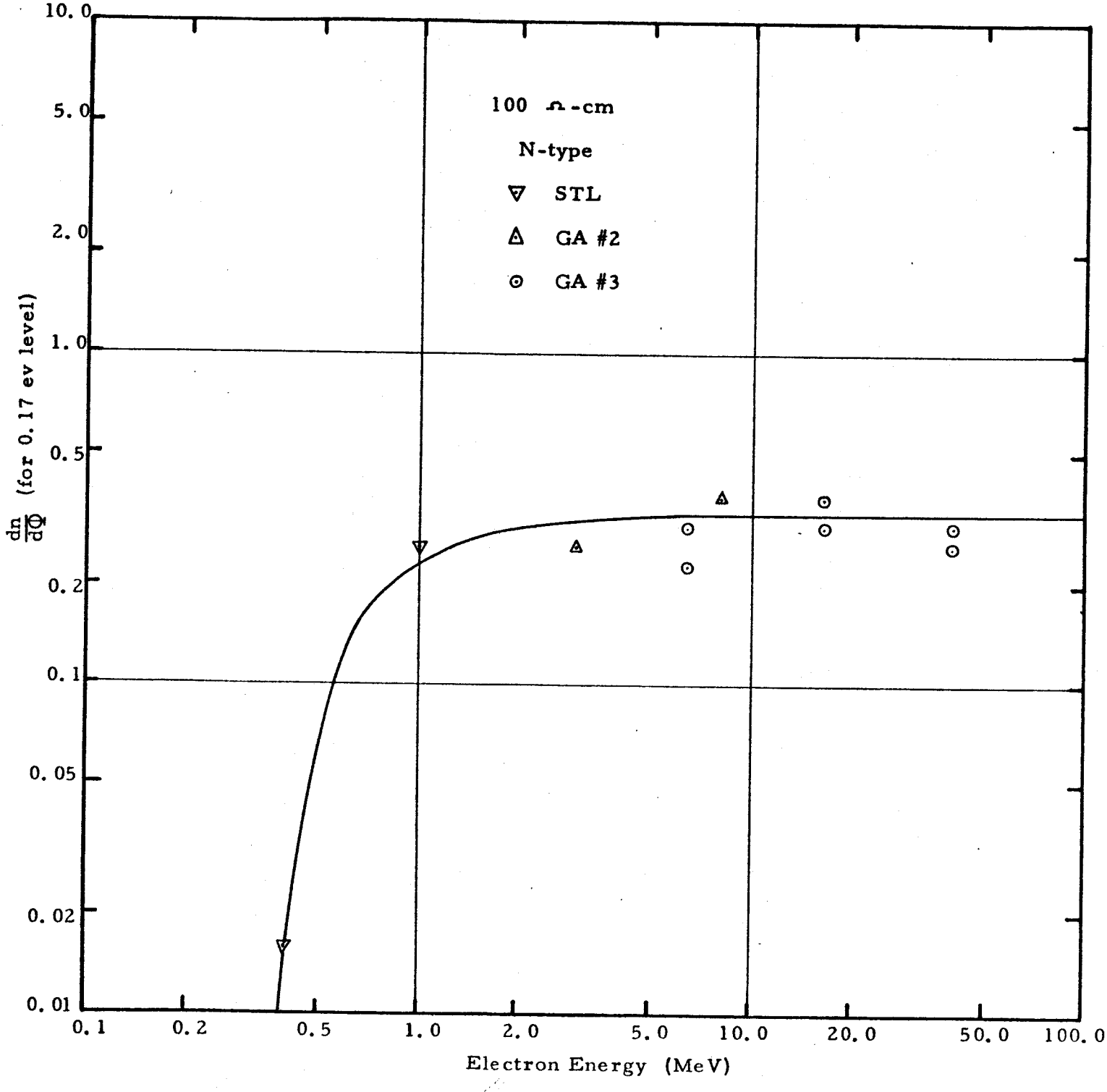

Figure 14. Electron Energy Dependence of the $E_c - E_t = 0.17$ ev Defect Level in 100 Ω-cm N-type Silicon

accomplished resulting in an accurate energy dependence function over the practical range of interest from 0.4 Mev to 40.0 Mev. Estimation of solar cell radiation damage and subsequent power supply degradation in space for n on p cells of any resistivity can be performed with the results of these experiments to an accuracy better than the knowledge of the radiation environment in space. It was also observed that the shape of the energy dependence curve of electron radiation damage in p-type silicon is independent of resistivity and, therefore, the difference in the absolute damage rates for any energy over the range of resistivities from 1.0 to 21.0 ohm-cm can be predicted quite accurately. As a result of these findings, it will be possible to do any further testing on n on p solar cells at 1.0 Mev and extrapolate the damage characteristics to other electron energies. This technique has several advantages in that the conduct of experiments at 1.0 Mev is an expedient and economical task and, further, the large number of 1 Mev Van de Graaff accelerators currently in operation relative to the higher energy linear accelerators renders this technique available to a large number of organizations.

The practical importance of the observed steep energy dependence for n on p solar cells lies in the integration of this energy dependence relationship with the fission beta energy spectrum of the artificial electron radiation belt. The result of the folding of the n on p silicon solar cell energy dependence with this fission electron energy spectrum is an increase in the predicted damage rate of approximately a factor of three over that predicted on the basis of the theoretical energy dependence as characterized by p on n solar cell response. Though the energy dependence of the more radiation resistant n on p cells is a much steeper function than the p on n cells, extrapolation of the damage rate versus energy characteristics

indicates that the n on p cell will remain superior to the p on n cell in radiation resistance to electron energies of beyond 1 Bev. Hence, even though the n on p cells suffer more rapidly increasing degradation under higher energy electrons than do p on n cells, their absolute sensitivity to radiation will always remain superior to the p on n cells at any electron energy of practical interest.

The theoretical analysis of the recombination statistics in electron degraded n on p solar cells indicates that an energy level 0.17 ev below the conduction band controls the recombination. This was confirmed by a study of the effect base resistivity on degraded lifetime and a study of degraded lifetime as a function of temperature. This energy level is believed to be associated with an oxygen-vacancy pair. Production of such a defect would probably be controlled by single displacements. It was shown, however, that while data for K and I_c versus E_b of p on n solar cell agree with single displacement theory, similar data for n on p cells do not. These data for n on p cells suggest that the controlling defect may result from a multiple displacement. In this respect, the damage rate studies disagree with the Hall, Shockley-Read data for n on p solar cells.

The Hall coefficient data for the energy dependence of defect introduction rate are roughly similar to the energy dependence of solar cell degradation. This is also in direct contradiction of the Hall, Shockley-Read recombination studies. Data acquisition and analysis are continuing in this area, and it is hoped that future results will aid in clarifying the situation. Once it is possible to pin down the energy levels responsible for minority carrier recombination, it will be possible to hypothesize models of defect structure and subsequently establish theoretical equations to explain the observed energy

dependence. Although adequate models and equations do not exist at this time, it appears that the energy dependence is not always controlled by the primary event of the displacement of a silicon atom from this lattice site by the incident high energy electron. The mechanism must, therefore, be related to either characteristics of secondary progeny displacement or transport of defects to sites where stable defect complexes with active energy levels are formed.

REFERENCES

1. J. M. Denney, R. G. Downing, G. W. Simon, and W. K. Van Atta, "Charged Particle Radiation Damage in Semiconductors, VI: The Electron Energy Dependence of Radiation Damage in Silicon Solar Cells," Report No. 8653-6019-KU-000, Contract NAS5-1851, (13 February 1963), TRW Space Technology Laboratories, Redondo Beach, California.

2. J. M. Denney and R. G. Downing, "Charged Particle Radiation Damage in Semiconductors, VIII: The Electron Energy Dependence of Radiation Damage in Photovoltaic Devices," Report No. 8653-6025-KU-000, Contract NAS5-1851, (15 July 1964), TRW Space Technology Laboratories, Redondo Beach, California.

3. R. Gremmelmaier, Proceedings of the IRE, 46, 1045, (1958).

4. J. M. Denney, R. G. Downing, W. I. Hoffnung, and W. K. Van Atta, "Charged Particle Radiation Damage in Semiconductors, V: Effect of 1 Mev Electron Bombardment on Solar Cells," Report No. 8653-6018-KU-000, Contract NAS5-1851, (11 February 1963), TRW Space Technology Laboratories, Redondo Beach, Calif.

5. G. K. Wertheim, "Electron Bombardment Damage in Silicon," Physical Review (June 1958), Vol. 110, No. 6, 1272.

6. J. A. Baiker, "Recombination and Trapping in Normal and Electron Irradiated Silicon," Physical Review (1 February 1963), Vol. 129, No. 3, 1174.

7. G. D. Watkins and J. W. Corbett, "Electron Paramagnetic Resonance of Defects in Irradiated Silicon," Discussions of the Faraday Society, (1961), No. 31 (87).

8. J. R. Carter and R. G. Downing, "Charged Particle Radiation Damage in Semiconductors, VII: Energy Levels of Defect Centers in Electron and Proton Bombarded Silicon," Report 8653-6021-KU-000, Contract NAS5-1851, (15 February 1963), TRW Space Technology Laboratories, Redondo Beach, California.

9. D. E. Hill, "Electron Bombardment of Silicon," Physical Review, (15 June 1959), Vol 114, No. 6, 1414.

10. G. Bemski and W. M. Augustyniak, "Annealing of Electron Bombardment Damage in Silicon Crystals," Physical Review, Vol. 108, No. 3, November, 1957.